Desalination and Water Treatment
www.deswater.com
doi: 10.5004/dwt.2018.22405

127 (2018) 313–324
September

Study on the adsorption/degradation of Rhodamine B by Fenton-like reagent based on carbon nanotubes

Ting Zhao[a,1], Min Yang[a,1], Mei Bai[b], Colin J. Barrow[c], Wenrong Yang[c], Wei Tan[a,*], Hongbin Wang[a,*]

[a]*School of Chemistry and Environment, Yunnan Minzu University, Kunming 650500, China, Tel. +86 13708440749; Fax: +86 0871 65910015; emails: 317266182@qq.com (W. Tan), wanghb2152@126.com (H. Wang), Tel. +86 14787820612; email: 1821157000@qq.com (T. Zhao), Tel. +86 18669010092; email: 826677468@qq.com (M. Yang)*
[b]*Key Laboratory of Resource Clean Conversion in Ethnic Regions, School of Chemistry and Environment, Yunnan Minzu University, Kunming 650500, China, Tel. +86 18669010092; email: 786432932@qq.com*
[c]*Centre for Chemistry and Biotechnology, School of Life and Environmental Sciences, Deakin University, Waurn Ponds, VIC 3216, Australia, Tel. +86 087165910017; email: colin.barrow@deakin.edu.au (C.J. Barrow), Tel. +613 5227 2932; email: wenrong.yang@deakin.edu.au (W. Yang)*

Received 15 October 2017; Accepted 25 April 2018

ABSTRACT

In this work, Rhodamine B (RhB) dye was catalytically degraded by using Fenton-like reagent (CNIQ), which was made by self-made multiwalled carbon nanotubes (MWNTs) supported iron oxide Fe_xO_y (MWNTs-Fe_xO_y) and H_2O_2. The MWNTs-Fe_xO_y was characterized by transmission electron microscope (TEM), energy dispersive spectrometer (EDS), Fourier transform infrared spectroscopy (FT-IR), Brunauer, Emmett, and Teller (BET), and X-ray photoelectron spectroscopy(XPS). The factors affecting the degradation of RhBs include the pH value, the reaction temperature, the dosage of MWNTS-Fe_xO_y, the dosage of H_2O_2, the treatment methods, and the concentration of RhB were investigated. Based on the TEM, EDS, FT-IR, BET, and XPS analysis, iron oxide was successfully loaded on carbon nanotubes. The RhB removal rate could reach to 100% under the optimal conditions: the solid to liquid ratio is 1:2, the amount of H_2O_2 (30%) is 0.1 mL, pH is 3.58, and oscillating time is 60 min. The results also show that the adsorption kinetic of RhB onto MWNTS-Fe_xO_y belongs to the pseudo-second-order kinetics. The activation energy and adsorption rate constant are 21.76 kJ/mol and 0.00047 g/(mg min), respectively, the degradation rate increases with the temperature increasing. From this study, we conclude that CNIQ has better adsorption/degradation effect for dye RhB, and it can be used widely in water treatment of textile industry.

Keywords: Carbon nanotubes; Iron oxide Fe_xO_y; RhB; Fenton reagent; Adsorption

1. Introduction

Multiwalled carbon nanotubes (MWNTs) special physical and chemical properties such as great specific surface area, stable chemical properties, heat resistance, corrosion resistance, and impact resistance [1] have aroused people's great attention. And it was widely used in reinforced composites [2,3], catalyst carrier [4,5], absorbent material separation [6,7], and some other fields in science like medicine and environment [8]. In Skandari's [9] experiment, oxidized carbon nanotubes (CNTs) were bound to the surface of silica sand through 3-(triethoxysilyl)propylamine to act as a bonding agent. The removal potential of humic acid with the new adsorbent was studied, according to the obtained data, CNTs have a good potential in the removal of humic acid (q_{max} = 81.96 mg/g CNT). Tran [10] with the recent well-documented ability to chemically modify nanofibrous carbon materials to improve

* Corresponding author.
[1]These authors contributed equally to this work.

their solubility and biocompatibility properties. Beyond that, series of positive research results have been achieved [11,12]. Therefore, CNT has a considerable application prospect especially in the field of the environment, for example, Chen [13] examined the interaction between Eu(III) and a multiwall carbon nanotube (MWCNT)/iron oxide magnetic composite in the absence and presence of poly(acrylic acid). The results are important for estimating and optimizing the removal of organic and inorganic pollutants by the magnetic composite. Cho [14] probed the influence that surface oxides exert on CNT sorption properties, and MWCNTs with varying oxygen concentrations were studied with respect to their sorption properties toward naphthalene. The results highlight the important role of surface chemistry in controlling the environmental properties of CNTs.

Due to the large amount of organic matter in the high temperature water will rapidly deplete the dissolved oxygen in the water, printing and dyeing wastewater can transform the natural water to anaerobic environment [15]. RhB, a pink color synthetic dye with high chromaticity, will block the sunlight into the water, reduce the photosynthesis of aquatic life, and then affect the growth of aquatic life. Because of its stronger toxicity and its poorer biochemical degradability, RhB can make the water color change after discharging into water, and destruct the natural ecosystem of water. At the same time, RhB also greatly reduce the economic value of water. Therefore, effective methods must be used for RhBs processing before being poured into water environment. Various methods have been developed and introduced to degrade RhB, such as the flotation method [16], flocculation precipitation, adsorption method [17], and catalytic oxidation method [18]. Among them, the Fenton reagent oxidation method has a broad application prospect, strong oxidizing and good degradation effect in environmental remediation. For example, Liu [19] studied the removal process of NO from SO_2-containing simulated flue gas using an ultraviolet (UV)/Fenton-like reaction in a photochemical reactor, and Guo [20] studied the removal of NO in a laboratory-scale bubbling reactor.

In this work, MWNTs-Fe_xO_y was prepared by the liquid-phase synthesis method and used Fenton-like reagent (CNIQ), for degradation of RhB. The adsorption/degradation performance of a single material and composite materials for RhB were investigated. The factors affecting the degradation of RhBs include the pH value, the reaction temperature, the dosage of MWNTs-Fe_xO_y, the dosage of H_2O_2, and the concentration of RhB were investigated, which can provide reference for the application of CNTs in the wastewater treatment.

2. Experimental

2.1. Materials and apparatus

Ferrous sulfate heptahydrate ($FeSO_4·7H_2O$, analytical reagent), natrium borohydride ($NaBH_4$), sodium hydroxide (NaOH), hydrochloric acid (HCl), RhB (Tianjin Wind Boat Chemical Reagent Technology Co. LTD, Tianjin, China), anhydrous ethanol (CH_3CH_2OH), hydrogen peroxide (H_2O_2), ethylene glycol ($(CH_2OH)_2$), and secondary distilled water. All the above reagents are analytical pure.

The morphology and the size of the materials were characterized by JEM-2100 transmission electron microscope (TEM; JEOL, Tokyo, Japan), Tecnai G2 TF30S-Twin energy dispersive spectrometer (EDS, FEI, Netherlands), Nicolit IS10 Fourier transform infrared spectroscopy (FT-IR, Thermo Scientific, Germany), D/max-2400 X-ray diffractometer (XPS (X-ray photoelectron spectroscopy), Ricoh, Japan), AUTOOR-1 Physical adsorption instrument (BET (Brunauer, Emmett, and Teller), Quantachrome, USA). Various degradation equipments were used in the adsorption/degradation of RhB experiment such as HQ45A-II thermostatic oscillator, 8453 UV-vis spectrophotometer instrument (Agilent, USA), pHS-3c pH meter, and the Type of 7200 visible spectrophotometer.

2.2. The preparation of MWNTs-Fe_xO_y

MWNTs-Fe_xO_y was prepared according to the liquid-phase synthesis method [21]. The reaction takes place in a flask with a circular bottom, and the processing parameters for MWNTs-Fe_xO_y preparation are shown in Table 1. $NaBH_4$ was chosen as reducing agent, and $FeSO_4·7H_2O$ was used as source of iron. Solution of $FeSO_4·7H_2O$ (0.18 mol/L) was prepared by dissolving $FeSO_4·7H_2O$ in ethanol–water solution (V/V = 3:7), and solution of $NaBH_4$ (0.36 mol/L) was prepared by dissolving $NaBH_4$ in ethanol–water solution (V/V = 3:7). The $FeSO_4·7H_2O$ solution was deoxidized by using nitrogen, then 2 mL polyethylene glycol 2000 (PEG2000) and 0.5 g CNTs were added. Finally, $NaBH_4$ solution was added into the mixed solution of $FeSO_4·7H_2O$ by using separating funnel. Nitrogen as a protection gas and introduced in a flask with a circular bottom to prevent oxygen entering, after reacting about 20 min, MWNTs-Fe_xO_y was washed by ultrapure water and anhydrous ethanol, and dried in vacuum oven at 50°C, then preserved in dry machine for next step. The shelf life of MWNTs-Fe_xO_y is 2 weeks, because iron will be oxidized and metamorphosed with time.

2.3. Adsorption/degradation of RhB

Series of (50–200 mg/L) RhB aqueous solution (pH = 1–13, adjusted by 1 mol/L NaOH and HCl) were prepared and adsorbent was added (MWNTs-Fe_xO_y). Second, the mixture was placed in the HQ45A-II thermostatic oscillator (25°C, 200 rpm) and oscillated for a certain time. Finally, the mixture was centrifuged. The supernatant was determined by using the type of 7200 visible spectrophotometer in the maximum absorption wavelength (555 nm), and ultrapure water was chosen as blank. The standard curve equation (the linear equation: $Y = 0.2109x - 0.007$, linear range: 0.5–4.5 mg/L, correlation coefficient: $r = 0.9997$) was used to calculate the concentration of RhB. The adsorption/degradation performance of MWNTs-Fe_xO_y on RhB was evaluated by the degradation rate and degradation amount.

Table 1
The processing parameters for MWNTs-Fe_xO_y preparation

Reagents	Concentration	Volume (mL)
$FeSO_4·7H_2O$	0.18 mol/L	50
$NaBH_4$	0.36 mol/L	50
PEG2000	30%	2

Adsorption/degradation rate (R(%)) was calculated using the following formula [22]:

$$R(\%) = \frac{C_0 - C_t}{C_0} \times 100\% \quad (1)$$

where R represents removal rate of RhB by MWNTs-Fe_xO_y (%), C_0 is the initial concentration of RhB in aqueous solution before adsorption (mg/L), and C_t is the residual concentration of RhB in aqueous solution at time after adsorption.

Adsorption/degradation amount (Q (mg/g)) was calculated using the following formula:

$$Q = \frac{(C_0 - C_t) \times V}{m} \quad (2)$$

where Q is adsorption capacity of RhB on MWNTs-Fe_xO_y (mg/g), m is mass of MWNTs-Fe_xO_y (mg), and V is volume of aqueous solution of RhB (mL).

2.4. Adsorption/degradation performance

Adsorption/degradation rate was used to evaluate the removal efficiency of MWNTs-Fe_xO_y. Many affecting factors on the adsorption/degradation performance were investigated, such as pH, temperature, dosage of MWNTs-Fe_xO_y, H_2O_2 dosage, initial concentration of RhB, and different treatment methods. The adsorption/decoloration kinetics were also studied.

3. Results and discussion

3.1. Characterization of MWNTs-Fe_xO_y

3.1.1. Morphology

In order to determine the ferric oxide whether it was loaded on MWNTs or not, TEM and scanning transmission electron microscopy (STEM) (or high-resolution transmission electron microscopy, HRTEM) were chosen for morphological analysis and the results were shown in Fig. 1 ((a) TEM, 50 nm, 30,000 times; (b) STEM, 50 nm, 80,000 times; (c) TEM, 200 nm, 30,000 times; and (d) HRTEM, 10 nm, 80,000 times). The TEM photos ((a) and (c))show that the surface of MWNTs is covered with a layer of needle-like material which would be Fe_2O_3. From STEM photos ((b) and (d)), many fine particles can be clearly observed on the tube wall, with the increase of iron/carbon ratio, and more particles can be seen. Therefore, we can confirm that the ferric oxide has been loaded onto the MWNTs.

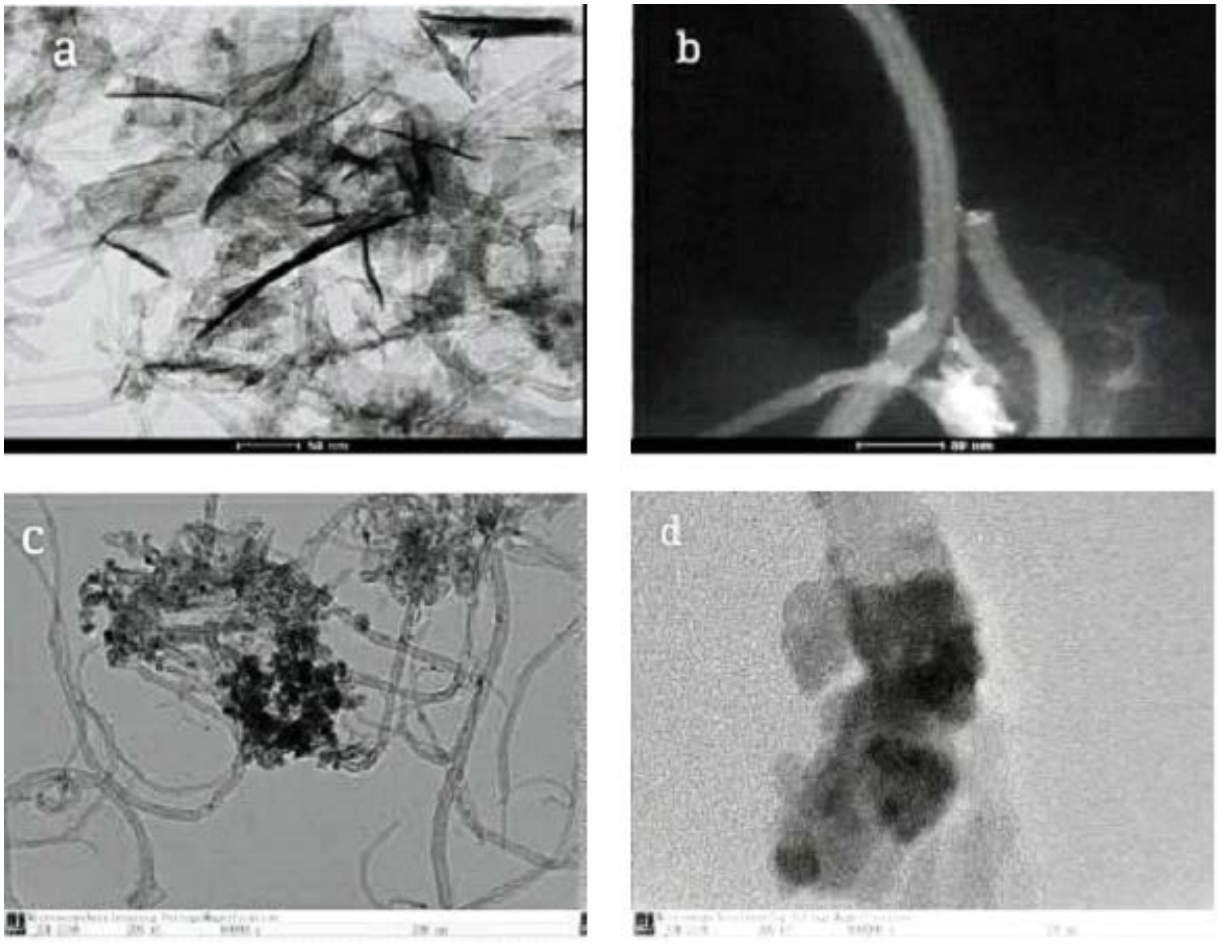

Fig. 1. Transmission electron microscope images of MWNTs-Fe_xO_y ((a) TEM, 50 nm, 30,000 times; (b) STEM, 50 nm, 80,000 times; (c) TEM, 200 nm, 30,000 times; and (d) HRTEM, 10 nm, 80,000 times).

3.1.2. Energy spectrum analysis

In order to ascertain that the iron oxide had been loaded successfully on MWNTs, EDS of MWNTs and MWNTs-Fe_xO_y is compared in Fig. 2. Based on the EDS, there are only energy peaks of the C and Cu in MWNTs (Fig. 2(a)) [23], and the copper would come from copper mesh, which was used for bearing MWNTs. From the figure of MWNTs-Fe_xO_y (Fig. 2(b)), except energy peaks of the C and Cu, we can also see the energy peaks of Fe that may produce by acicular Fe_2O_3 and spherical Fe_3O_4. Therefore, we can confirm Fe is successfully loaded on the MWNTs.

3.1.3. FT-IR spectrum

The data of precise molecular structure information were recorded by FT-IR which spectra were shown in Fig. 3 and Table 2. We found that the intensity of absorption peak at 614 cm^{-1} (Fig. 3(b)) is presented, this may be contributed by the contraction vibration peak of Fe–O in Fe_3O_4 [24]. As a result of the embedded water of MWNTs-Fe_xO_y, the intensity of peak at 3,450 cm^{-1} (in Fig. 3(b)) is weaker than the peak at 3,453 cm^{-1} (in Fig. 3(a)), and shifted to lower wave number after loaded. It is obvious that the absorption peak of MWNTs from 2,360.38 cm^{-1} move to 2,331 cm^{-1}, it could be the triple bond contraction vibration peak or the CO_2 gas was taken when the samples were removed rapidly, so the O=C=O stretching vibration peak was appeared in samples. The peak at 1,645 cm^{-1} belongs to stretching vibration of C=C, which comes from the ports of MWNTs or the damaged five-membered ring and seven-membered ring [25]. The bands at 1,456, 1,264, 1,123, and 1,070 cm^{-1} are attributed to the C–C skeleton vibration, and near 858 and 550 cm^{-1} are impurity peaks of MWNTs.

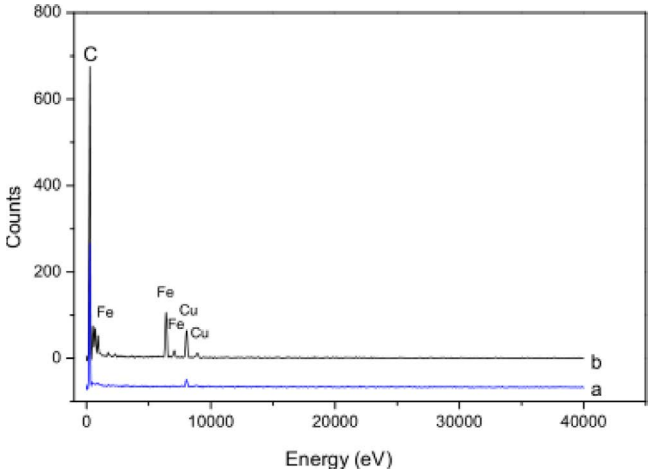

Fig. 2. EDS images of MWNTs (a) and MWNTs-Fe_xO_y (b).

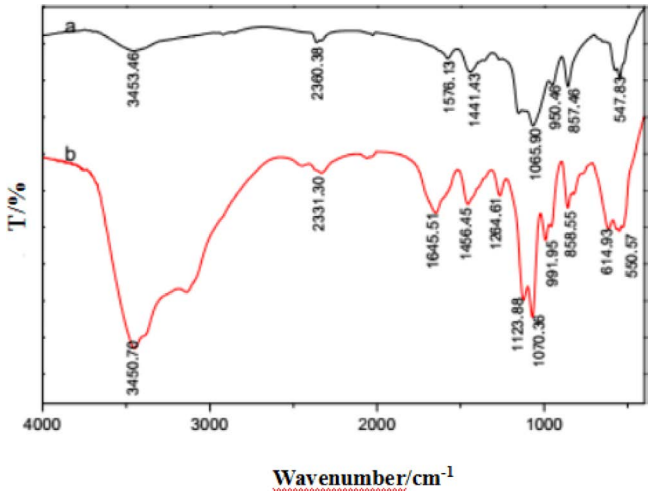

Fig. 3. FT-IR spectra of MWNTs (a) and MWNTs-Fe_xO_y (b).

Table 2
The FT-IR analysis of MWNTs and MWNTs-Fe_xO_y (cm^{-1})

Samples	Fe–O	O–H	C≡C	C=C	C–C
MWNTs-Fe_xO_y	614	3,450	2,331	1,645	1,070–1,456
MWNTs	–	3,453	2,360	–	1,065–1,076

3.1.4. XPS analysis

The XPS pattern about the MWNTs-Fe_xO_y is given in Fig. 4, and the data of XPS are shown in Table 3. It shows that the iron is successfully loaded onto the CNTs. The XPS patterns from MWNTs-Fe_xO_y contain small diffraction peaks from Fe. Therefore, all the Fe is in the form of MWNTs-Fe_xO_y, most of the Fe is in the Fe^{2+} state.

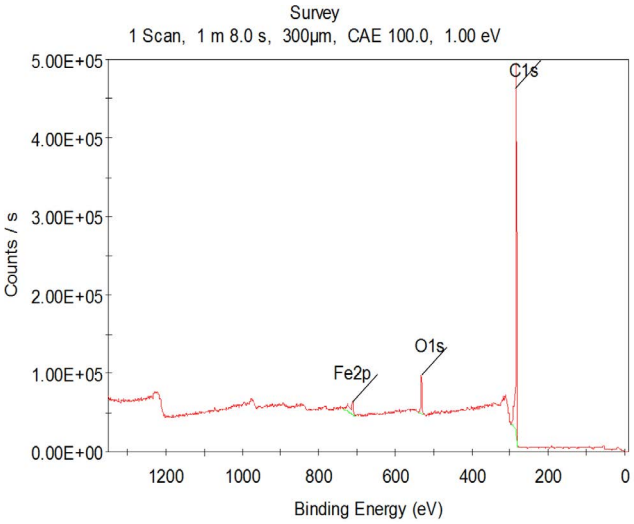

Fig. 4. XRD patterns of MWNTs-Fe_xO_y.

Table 3
The XPS analysis of MWNTs-Fe_xO_y (eV)

Binding energies	710	711	535	284	285	531
Chemical valence	Fe^{2+}	Fe^{3+}	–	–	–	–
Functional groups	Fe–O	Fe–O	H_2O	C–C	C=C	C–O

3.1.4.1. The XPS spectrum of Fe 2p for the MWNTs-Fe_xO_y

Initial XPS measurements were carried out on the Fe 2p peaks of MWNTs-Fe_xO_y. The XPS peaks of Fe $2p_{3/2}$ and Fe $2p_{1/2}$ for the MWNTs-Fe_xO_y are shown in Fig. 5. One of the two peaks Fe $2p_{3/2}$ peak is narrower and stronger than Fe $2p_{1/2}$. The area of Fe $2p_{3/2}$ peak is greater than that of Fe $2p_{1/2}$ because in spin–orbit (*j*–*j*) coupling, Fe $2p_{3/2}$ has degeneracy of four states while Fe $2p_{1/2}$ has only two [26]. The Fe $2p_{3/2}$ peak has associated satellite peaks. The satellite peak of Fe $2p_{3/2}$ for MWNTs-Fe_xO_y is located approximately 8 eV higher than the main Fe $2p_{3/2}$ peak [27]. The satellite peak at 718.8 eV (S.D. = 0.13) is clearly distinguishable and does not overlap either with Fe $2p_{3/2}$ or Fe $2p_{1/2}$ peak. In addition, there appears to be another satellite peak at 729.5 eV and this may be a satellite peak for Fe $2p_{1/2}$.

3.1.4.2. The XPS spectrum of Fe 3p for the MWNTs-Fe_xO_y

The XPS spectrum of Fe 3p for the MWNTs-Fe_xO_y is shown in Fig. 6. Although the Fe 3p peak consists of both Fe $3p_{3/2}$ and Fe $3p_{1/2}$, a single peak was observed in the XPS spectrum obtained from this study. This separation energy of the XPS peaks is proportional to the spin–orbit coupling constant, which depends on the value $h1/r^3$ (where r is a radius) for the particular orbit [28]; treating the Fe 3p peak as a single peak, the physical parameters, that is, peak position, full width at half maximum, asymmetry factor, and Gaussian–Lorentzian ratio of the Fe 3p peak for Fe^{3+} were determined from the spectrum. The curve fitting was carried out using the GL ratio = 40 (Gaussian:Lorentzian = 60:40), the symmetry factor of 0.4, and linear background subtraction between 62 and 50 eV which gave the smallest x^2 [29].

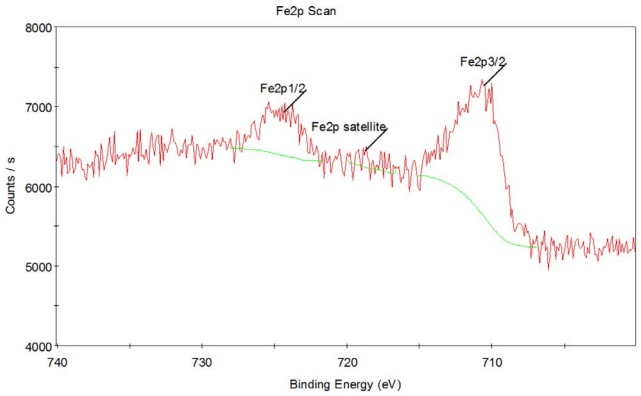

Fig. 5. The XPS spectrum of Fe 2p from the fractured surface of the MWNTs-Fe_xO_y.

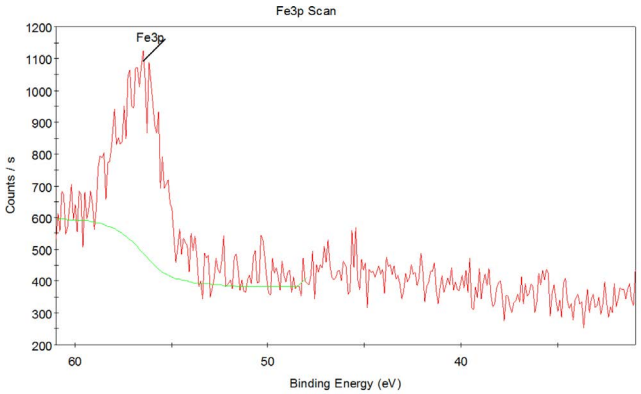

Fig. 6. The XPS spectrum of Fe 3p from the fractured surface of the MWNTs-Fe_xO_y.

3.1.4.3. The XPS spectrum of C1s and O1s for the MWNTs-Fe_xO_y

Carbon is found in all surfaces of XPS analysis. It is common practice to use the carbon C1s peak at 285 eV as a reference for charge correction. In routine XPS, analyses of samples prepared outside the high vacuum chamber relatively thick carbon layers are formed on the surfaces, and the corrected XPS peak positions are independent of the apparent or experimentally obtained binding energy. The reason why the corrected C1s position is a function of the experimentally obtained C1s peak position is not clear. Therefore, the C1s peak is not the suitable reference peak. Instead, the O1s peak was used as the reference for the charge correction in this study. It shows the corrected Fe $2p_{3/2}$ peak position to be independent of experimentally obtained O1s peak position within experimental uncertainties. Some of the factors influencing peak position in these systems have been discussed by the authors [30]. Therefore, since C1s peak is not suitable for charge correction, the O1s peak with the binding energy of 530.0 eV was used for the charge correction throughout this study. The typical C1s (Fig. 7(a)) peaks and O1s (Fig. 7(b)) for MWNTs-Fe_xO_y are, respectively, shown in Fig. 7.

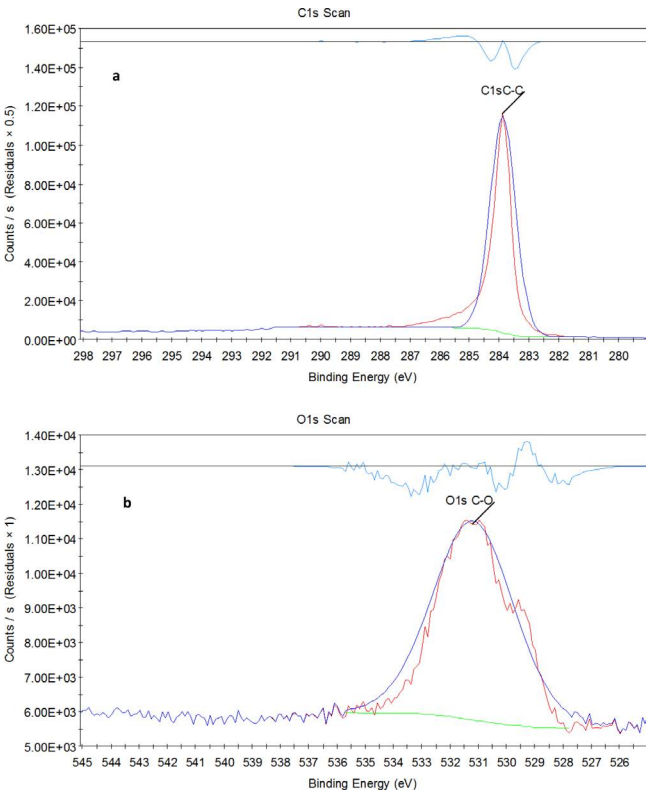

Fig. 7. The XPS spectrum of C1s (a) and O1s (b) for the MWNTs-Fe_xO_y.

3.1.5. BET analysis

The BET analysis of MWNTs and MWNTs-Fe_xO_y is shown in Table 4 [31]. As shown in Table 4, the surface area decreased from 95.509 m^2/g (in MWNTs) to 75.060 m^2/g (in MWNTs-Fe_xO_y). The reason could be that the surface of the CNT is occupied by iron oxide. At the same time, average pore width increased from 1.213 nm (in MWNTs) to 1.418 nm (in MWNTs-Fe_xO_y). In addition, we can see that the total pore volume of CNTs increased about six times after loaded by iron oxide. This can improve the adsorption capacity of MWNTs-Fe_xO_y.

3.2. Optimizing the adsorption/degradation conditions

3.2.1. pH

In order to investigate the effect of pH, the experiment was carried out at different solution pH value ranging from 2 to 12. As shown in Fig. 8, the degradation rate and the degradation capacity of RhB reached 99% and 203 mg/g, respectively, in acidic environment. The removal rate gradually decreases when the pH value increases, the reason is that MWNTs can produce hydroxyl radicals in the Fenton reaction, which has stronger oxidation ability. The pH of RhB wastewater is around 3.58 when its concentration is 100 mg/L, so the original pH was chosen in this experiment.

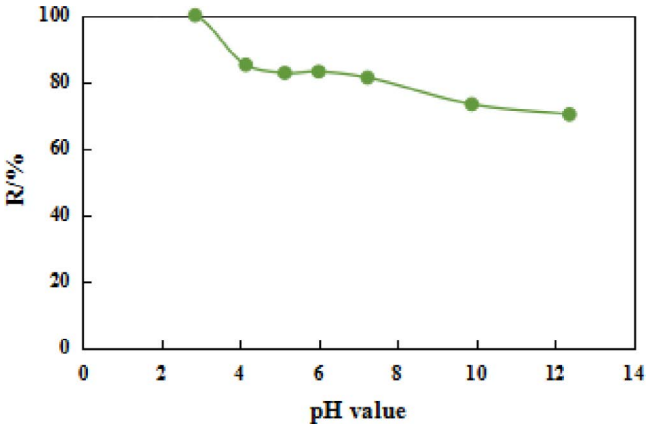

Fig. 8. Effect of pH value on the removal rate of Rhodamine B.

3.2.2. Reaction temperature

The effects of the different temperature were researched and the results are shown in Fig. 9. It can be seen that higher temperature is favorable for the degradation of RhB, the removal rate of RhB reached to 90% at 150 min when the reaction temperature was 17°C, and the removal rose of RhB reached to 99% after 60 min when the reaction temperature was increased to 25°C, 35°C, 45°C, the residual concentrations of RhB gradually decreased with the reaction temperature increasing. Because the decomposed velocity of H_2O_2 is faster in higher temperature, which leads •OH free radicals increased in the solution, so higher temperature is benefitted to accelerate the rate of adsorption/degradation, and improve the removal rate of RhB significantly.

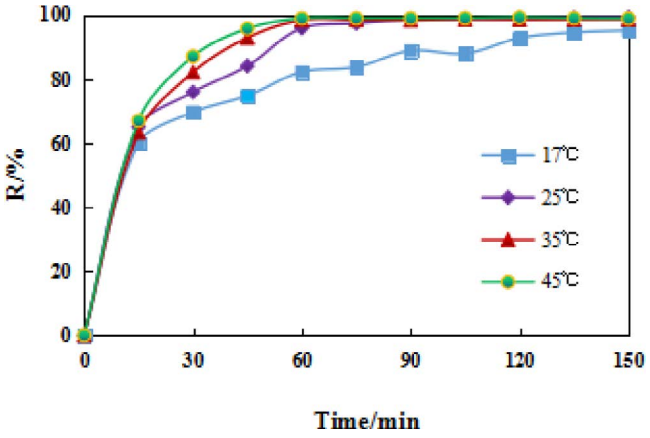

Fig. 9. Effect of reaction temperature on the removal rate of Rhodamine B.

3.2.3. The effect of adsorbent dosage

In order to investigate the optimum adsorbent dosage, the adsorption/degradation of RhB in different amount of catalyst was examined and the results are shown in Fig. 10. It can be seen that the performance of degradation under the same conditions is: the MWNTs-Fe_xO_y + H_2O_2 > MWNTs-Fe_xO_y > the oxidation of MWNTs, H_2O_2 can promote the reaction efficiency, the reason could be that the blocked channels of MWNTs would be opened by H_2O_2, at the same time, the MWNTs-Fe_xO_y and H_2O_2 formed the Fenton system. The degradation/adsorption rate reaches 95% when 25 mg materials was added in 50 mL RhB solution, and then the degradation/adsorption rate tend to balance with the amount of MWNTs-Fe_xO_y increasing. Therefore, based on the economic consideration, the the optimal conditions were: the volume and concentration of RhB aqueous solution were 50 mL and 100 mg/L, respectively, the amount of MWNTS-Fe_xO_y was 25 mg.

3.2.4. The effect of H_2O_2

The influence of H_2O_2 amount is shown in Fig. 11, it can be seen that the removal rate of RhB increases with H_2O_2 amount increasing when H_2O_2 dosage is less than 0.1 mL. The removal rate of RhB mainly depended on the adsorption

Table 4
The BET analysis of MWNTs and MWNTs-Fe_xO_y

Samples	Surface area (m^2/g)	Micropore surface area (m^2/g)	Total pore volume (cm^3/g)	Pore volume (cm^3/g)	Micropore volume (cm^3/g)	Average pore width (nm)
MWNTs-Fe_xO_y	75.060	75.060	2.441	0.026	0.029	1.418
MWNTs	90.792	95.509	0.419	0.573	0.037	1.213

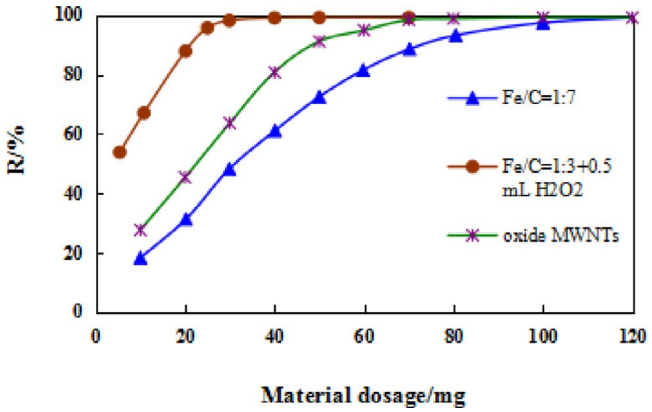

Fig. 10. Effect of immobilizing amount of MWNTs-Fe_xO_y on the removal rate of Rhodamine B.

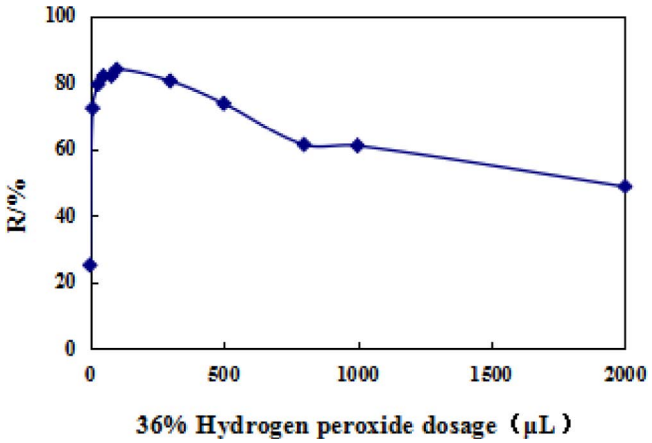

Fig. 11. Effect of immobilizing amount of H_2O_2 on the removal rate of Rhodamine B.

effect of MWNTs-Fe_xO_y when the amount of the H_2O_2 was 0 mL. But the removal rate declines with the increase of H_2O_2 when its dosage is more than 0.1 mL, even though it was maintained at a higher processing efficiency. This is probably because the amount of •OH radicals was increased with the increase of H_2O_2 dosage under the lower concentration, but one conclusion which comes from Li et al. [32] was that the •OH radicals were decreased when the concentration of H_2O_2 is higher than the critical value. Under these conditions, H_2O_2 is not only generating agent but also inhibitors for •OH, excess •OH free radicals should be converted to HO_2•, and then the treatment effect was declined with the reduction of •OH radicals. Related reactions are listed as follows:

$$H_2O_2 + {}^{\bullet}OH \rightarrow HO_2{}^{\bullet} + H_2O \quad (a)$$

$$HO_2{}^{\bullet} + {}^{\bullet}OH \rightarrow H_2O + O_2 \quad (b)$$

$$2{}^{\bullet}OH \rightarrow H_2O_2 \quad (c)$$

Therefore, the amount of H_2O_2 should be controlled within a certain range, and 0.1 mL 36% H_2O_2 was chosen as the best dosage in this experiment.

3.2.5. Concentration of RhB

The effects of different initial concentration of RhB are shown in Fig. 12. MWNTs-Fe_xO_y has better treatment efficiency for RhB when the initial concentration was in the range of 50–200 mg/L. The RhB's residual concentration was lower with the extension of reaction time, and the removal rate approached 100%. But the removal rate was declined when the initial concentration increased, the possible reason is that the quantity of •OH radicals were not enough to completely interrupt the chromophores in RhB aqueous solution. Second, the effective reaction mainly occurs on the catalysts surface area where the •OH radical can only exist less than 1 ns. When the concentration of RhB increased, more active sites on the surface of the catalysts were occupied, so the moving rate of H_2O_2 to catalysts surface and generating rate of •OH radicals were reduced, and then the •OH free radicals lose oxidation ability rapidly, therefore, the removal efficiency of RhB was reduced. In conclusion, the 100 mg/L of RhB aqueous solution was chosen as the optimal concentration.

3.2.6. The effect of treatment methods

In order to verify the best processing methods, three different methods on degrading RhB were designed: (1) 0.1 mL H_2O_2, (2) 25 mg MWNTs-Fe_xO_y, and (3) 0.1 mL H_2O_2 and 25 mg MWNTs-Fe_xO_y were added in three groups of Erlenmeyer flask which have 50 mL and 100 mg/L RhB aqueous solution, respectively. As shown in Fig. 13, the different treatment methods show obvious differences on the removal efficiency of RhB. The removal rate was only 5% when adding hydrogen peroxide alone, the oxidation ability of H_2O_2 was low and there was no catalyst action at this time, so the complex dye molecules such as RhB cannot be oxidized completely. The removal effect was only 32% when MWNTs-Fe_xO_y was added alone. But when 0.1 mL H_2O_2 and 25 mg MWNTs-Fe_xO_y were added in RhB aqueous solution, the removal rate reached to 100%, and it can be considered that CNIQ was formed. The •OH radicals are formed because the irons reacted with hydrogen peroxide in Fenton reaction, and the decrease of iron ion made •OH radicals increase in solution [33], therefore, 0.1 mL

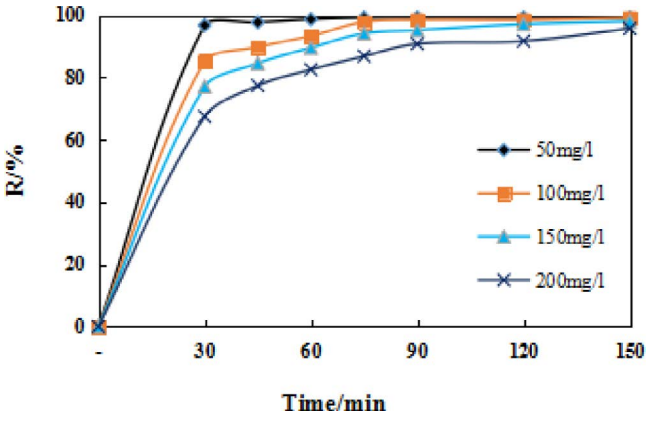

Fig. 12. Effect of initial concentration of Rhodamine B on the removal rate.

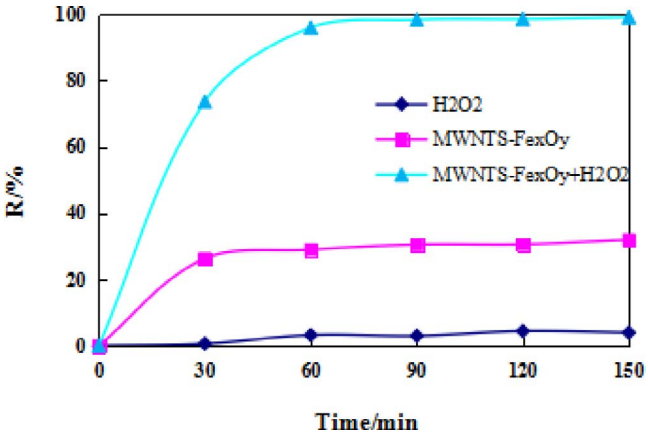

Fig. 13. Degradation of Rhodamine B under different experimental conditions.

H_2O_2 and 25 mg MWNTs-Fe_xO_y were chosen as optimal concentration.

3.3. Dynamic and thermodynamics

3.3.1. Adsorption kinetics

The pseudo-first-order rate equation can be satisfactorily described that the adsorption rate was determined by the number of free adsorption sites on the adsorbent surface, the pseudo-second-order kinetics mode can be used to describe that the rate of adsorption was determined by the square value of the number of vacancies on the surface of the adsorbent [34]. In this work, a series of kinetic studies [35] were performed to compare the adsorption/degradation rates of RhB, different systems and different influence factors such as reactant temperature and reaction concentration were studied in the kinetics experiments (Fig. 14), the parameters that define the two models tested (quasi-level 1 and quasi-level 2 dynamic models) were determined by fitting them to the experimental measurement (Table 5). The relevant numerical value was calculated using the following formula:

$$\ln\frac{(q_e - q_t)}{q_e} = -k_1 t \tag{3}$$

$$\frac{t}{q_t} = \frac{1}{k_2 q_e^2} + \frac{1}{q_e} t \tag{4}$$

where q_e and q_t (mg/g) represent the adsorption amount of triazophos adsorbed at equilibrium and at t time, respectively. k_1 (min^{-1}) and k_2 (g/(mg min) are the pseudo-first-order constant and pseudo-second-order constant, respectively.

In first-order kinetics, the values of correlation coefficient R did not exceed 0.998. It shows that the first-order kinetics is not reliable for explaining the kinetics of adsorption/degradation process. According to the results, the best fitting ($R \geq 0.9986$) was achieved for the level 2 dynamic model. The deviation between the actual capacity and fitting capacity is less than that of the fit of first-order kinetic, so that the secondary dynamics can describe the degradation reaction

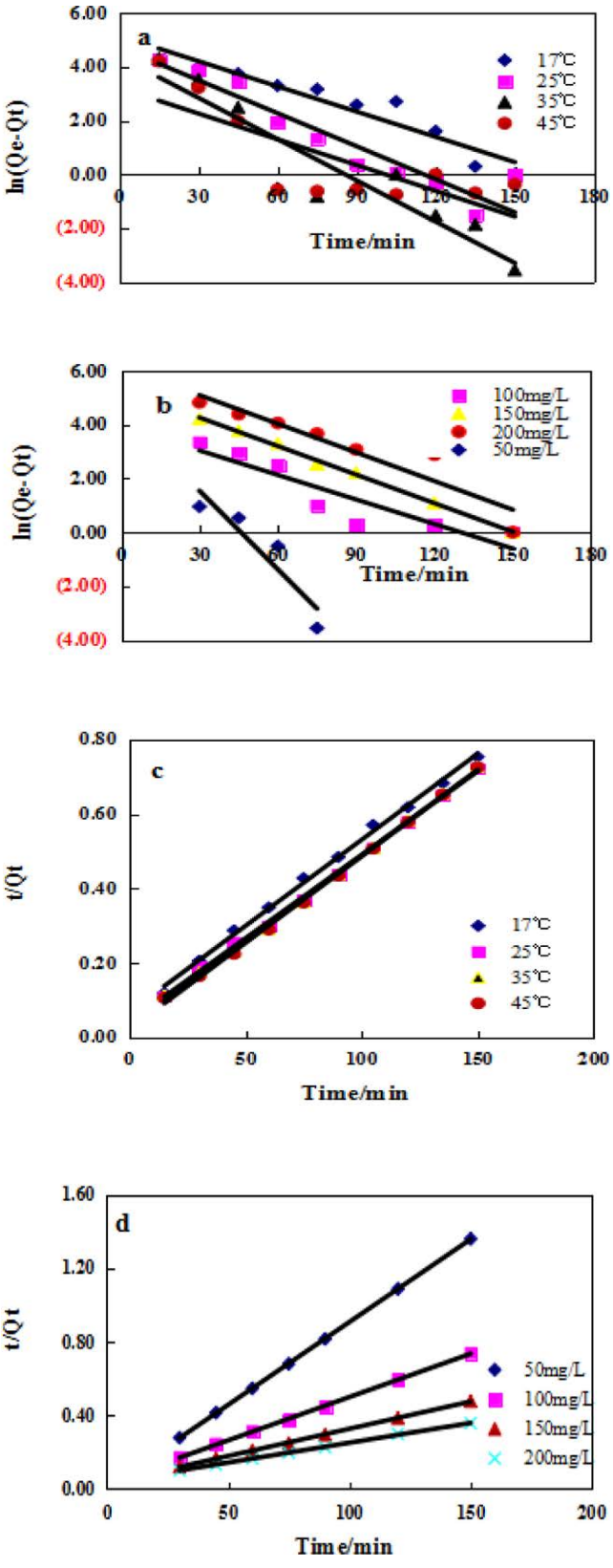

Fig. 14. Linear fitting of pseudo-first-order kinetics equation under different temperature (a) and different concentrations (b), and linear fitting of pseudo-second-order kinetics equation under different temperature (c) and different concentrations (d).

Table 5
Pseudo-first-order and pseudo-second-order kinetic equations of related parameter

Variable		Measued Q_e (mg/g)	Pseudo-first-order kinetic equations			Pseudo-second-order kinetic equations			
			Q_e (mg/g)	k_1 (min^{-1})	R	Q_e (mg/g)	h (mg/(g min))	k_2 (g/(mg min))	R
Concentrations of Rhodamine (mg/L)	50	110.42	86.42	0.0973	0.9240	111.11	140.85	0.01140	1.0000
	100	203.13	51.83	0.0304	0.9101	217.76	34.84	0.00073	0.9997
	150	314.09	204.75	0.0354	0.9984	333.33	32.26	0.00029	0.9998
	200	420.05	471.44	0.0355	0.9394	476.19	27.78	0.00012	0.9996
Temperature (K)	290	198.98	172.83	0.0313	0.9547	217.39	14.45	0.00031	0.9986
	298	207.42	113.90	0.0410	0.9440	222.22	23.15	0.00047	0.9990
	308	206.25	80.15	0.0512	0.9273	217.39	33.56	0.00071	0.9991
	318	207.42	25.02	0.0319	0.7829	217.39	44.64	0.00094	0.9993

Note: where Q_e, k_1, k_2, and h represent the equilibrium adsorption quantity, pseudo-first-order adsorption rate constant, pseudo-second-order adsorption rate constant, and initial adsorption rate constant, respectively.

process better and the adsorption of RhB is an endothermic process.

3.3.2. Degradation kinetics

The parameters of degradation kinetics are fitted with Arrhenius equation [36]. The $\ln(C/C_0)$ was seemed as the ordinate and time was seemed as the abscissa. When the graph line passes through the origin, the slope is $-K$, the half-life $t_{1/2}$ is obtained by K. The thermal degradation reaction constant K of 290, 298, 308, and 318 K was taken logarithm, the slope was E_a/R, and the vertical intercept was $\ln K_0$. The correlation formula was as follows:

$$\ln(C/C_0) = \ln(A/A_0) = -K_t \quad (5)$$

$$t_{1/2} = -\ln 0.5 \times K^{-1} \quad (6)$$

$$\ln K = \ln K_0 - E_a/RT \quad (7)$$

where C_0 is the initial concentration of RhB in aqueous solution before adsorption (mg/L) and C is the residual concentration of RhB in aqueous solution at time after adsorption. K represents the degradation constant, min^{-1}; K_0 represents the equation constant, min^{-1}; E_a represents the activation energy of kJ/mol; T represents the reaction temperature, K; and R represents the gas constant 8.314 J/(mol K).

The RhB content measured in the range of 290, 298, 308, and 318 K was calculated and shown in Figs. 15 and 16. According to Fig. 15, the correlation coefficient R^2 at each temperature is greater than 0.96, which indicates that the linearity is good and it accords with the first-order degradation kinetics. The thermal degradation reaction constant K of RhB is obtained from the curve equation in Fig. 16, and the degradation parameters are obtained as shown in Table 6. It can be seen that the degradation reaction constant K with the temperature increasing, while the half-life $t_{1/2}$ decreased, which is that RhB degradation accelerates with the increase of temperature. In other words, RhB degradation increases with temperature.

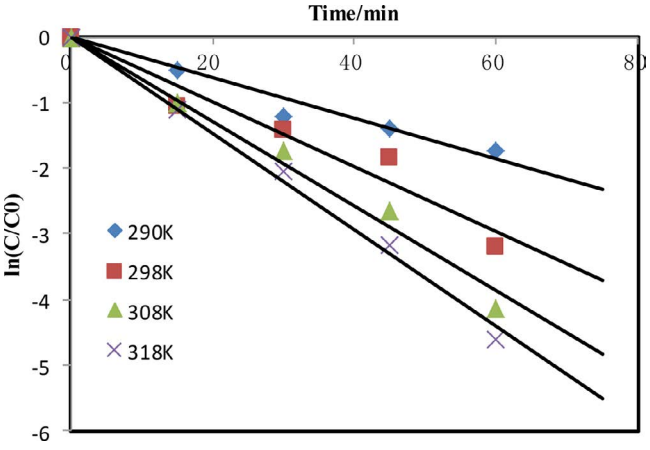

Fig. 15. Change of $\ln(C/C_0)$ with time at different temperatures.

Table 6
The thermal degradation kinetic parameters of RhB at different temperatures

T (K)	K	$t_{1/2}$ (min)	E_a (kJ/mol)	$\ln K_0$
290	0.031	22.26		
298	0.049	14.08	21.76	5.71
308	0.0645	10.69		
318	0.0737	9.36		

3.3.3. Thermodynamics

The mechanism of adsorption isotherm and adsorption isotherm is studied in this paper. In this study, two classical adsorption models were adopted: Langmuir and Freundlich [37]. The correlation formulas were as follows:

$$\text{Langmuir: } C_e/Q_e = C_e/Q_m + 1/bQ_e \quad (8)$$

where Q_m is the maximum adsorption capacity of single-molecule adsorption layer (mg/g) for particle surface,

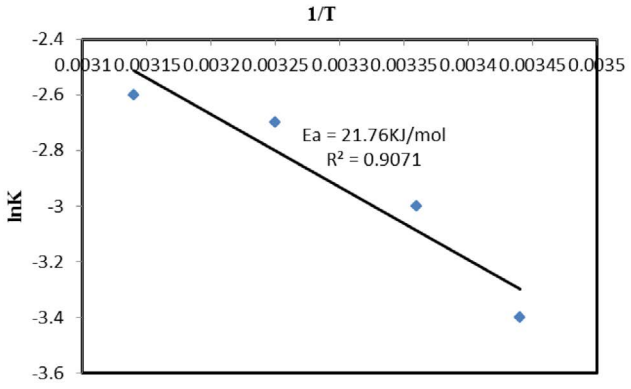

Fig. 16. Change of ln*K* with different temperatures.

Q_e is the equilibrium adsorption (mg/g), C_e is the equilibrium mass concentration (mg/L), and b is the Langmuir constant (L/mg).

Freundlich: $\log Q_e = \log k + (1/n)\log C_e$ (9)

where Q_e is the equilibrium adsorption (mg/g), C_e is the equilibrium mass concentration (mg/L), b is the Langmuir constant (L/mg), n is the empirical constant relating to temperature, and k is the Freundlich adsorption equilibrium constant.

The model fitting parameters of RhB adsorption on MWNTs-Fe$_x$O$_y$ are listed in Table 7. By comparing the correlation coefficient, the Freundlich model can well fit the adsorption of MWNTs-Fe$_x$O$_y$ to RhB, and the correlation coefficient R^2 is greater than 0.9988.

Adsorption isotherm under different temperature (a) and different concentrations (b) is shown in Fig. 17, the adsorption amount decreases with the increase of temperature, which is due to the adsorbed material density increased with increasing temperature decreased resulting in the decrease of average adsorption capacity. In addition, with the increase of RhBs concentration, the surface active sites of the adsorbent were quickly occupied. Therefore, the adsorption capacity decreases with the increase of concentration.

3.4. Regeneration experiment

The saturated adsorption MWNTs-Fe$_x$O$_y$ was regenerated repeatedly with anhydrous ethanol, the effect of regeneration frequency on regeneration efficiency is shown in Fig. 18. It can be found that the removal rate of adsorption material remains above 89% after multiple adsorption and regeneration. It shows that MWNTs-Fe$_x$O$_y$ has good recycling value.

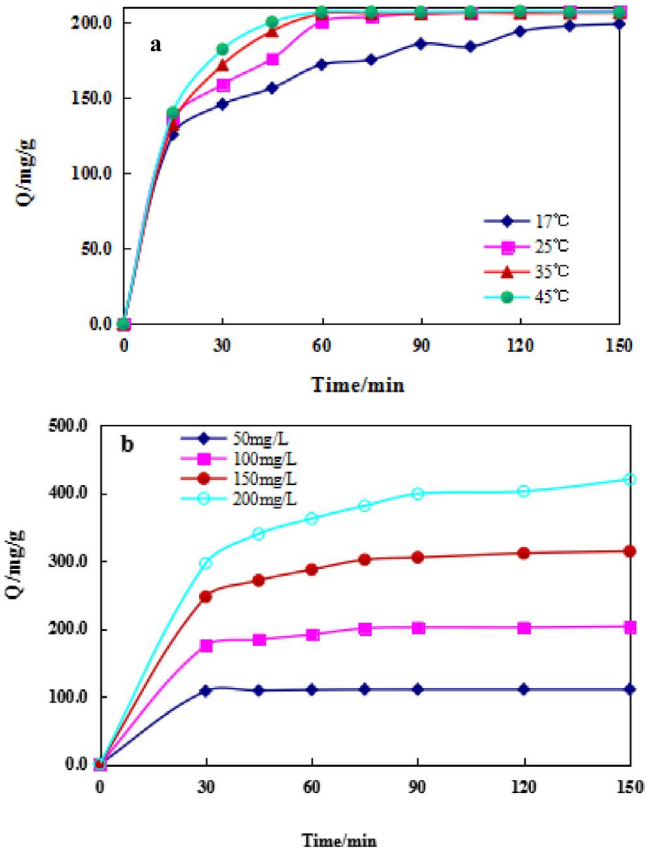

Fig. 17. Adsorption isotherm under different temperature (a) and different concentrations (b).

3.5. Discussion of mechanism

The color of dye in dyeing wastewater originates from the conjugate system of dye molecules, namely chromophore. Chromophore is a chromogenic system containing unsaturated groups (N=N, C=C, N=O, C=O, –NO_2). During the removal of RhB, it was obvious that the color of RhB solution was changed from yellow to colorless; it shows that the chromogenic group phenylamino and the carbonyl bond are destroyed gradually. Data [38] showed that RhB produced rhodamine during the removal process. The hydroxyl radical produced by Fe^{2+} and H_2O_2 in acidic condition breaks

Table 7
Adsorption isothermal model and parameters

T (K)	Langmuir ($C_e/Q_e = C_e/Q_m + 1/bQ_e$)				Freundlich ($\log Q_e = \log k + (1/n)\log C_e$)			
	Equation	Q_{max} (mg/g)	K_L (L/mg)	R	Equation	$1/n$	K_F	R
290	$Y = 0.0106x + 0.0041$	94.33	0.3868	0.8313	$Y = 0.2683x + 4.2214$	0.2683	68.1288	0.9387
298	$Y = 0.0054x + 0.0037$	185.19	0.6852	0.9106	$Y = 0.2656x + 4.4687$	0.2656	87.2432	0.9688
308	$Y = 0.0027x + 0.0025$	370.37	0.9259	0.9133	$Y = 0.3289x + 4.7511$	0.3289	115.712	0.9719
318	$Y = 0.003x + 0.0016$	333.33	0.5333	0.9620	$Y = 0.4082x + 5.2477$	0.4082	190.129	0.9575

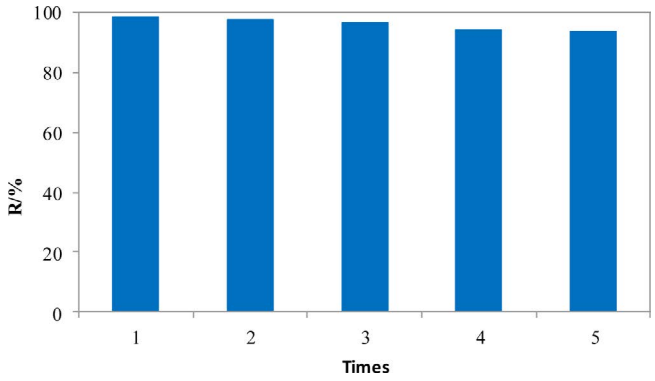

Fig. 18. Effect of regeneration times on adsorption.

the structure of conjugated system, and the colorless organic molecule was formed [39]. This is the main mechanism of degradation and decolorization of dyeing wastewater by Fenton oxidation reaction. The equations are as follows:

$$Fe^{2+} + H_2O_2 \rightarrow Fe^{3+} + OH^{\bullet} + OH^{-} \quad (d)$$

$$Fe^{2+} + OH^{\bullet} \rightarrow Fe^{3+} + OH^{-} \quad (e)$$

$$OH^{\bullet} + H_2O_2 \rightarrow HO_2^{\bullet} + H_2O \quad (f)$$

$$Fe^{2+} + HO_2^{\bullet} \rightarrow Fe(HO_2)^{2+} \quad (g)$$

$$Fe^{3+} + HO_2^{\bullet} \rightarrow Fe^{2+} + O_2 + H^{+} \quad (h)$$

$$HO_2^{\bullet} \rightarrow O_2^{-} + H^{+} \quad (i)$$

$$Fe^{3+} + O_2^{-} \rightarrow Fe^{2+} + O_2 \quad (j)$$

$$HO_2^{\bullet} + HO_2^{\bullet} \rightarrow H_2O_2 + O_2 \quad (k)$$

$$HO_2^{\bullet} + H_2O_2 \rightarrow H_2O + O_2 + {}^{\bullet}OH \quad (l)$$

In the reaction (d), the reaction between Fe^{2+} and H_2O_2 is very fast [40], and the hydroxyl radical was formed, which has a high electrode potential, and the oxidation ability is second only to fluorine. The $HO_2^{\bullet}$ formed in the reaction (h) can continue to perform the reaction shown in formula (l) [41].

In conclusion, the removal mechanism of RhB may be as follows: first, the chromogenic group phenylamino and the carbonyl bond in RhB are destroyed gradually, and the colorless organic intermediate was formed, so the color of RhB solution was changed to colorless. In the process of reaction, part of RhB can also be transformed into colorless lactone isomer (Fig. 19), which also reduces the color of solution. And then the colorless intermediates were degraded.

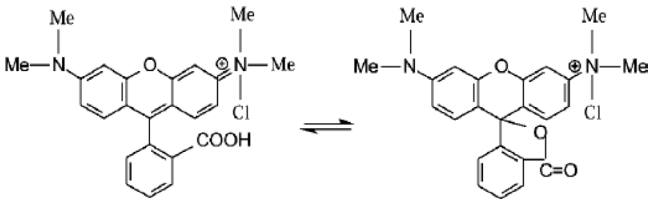

Fig. 19. Rhodamine B and its isomers.

4. Conclusions

In this study, we presented the synthesis of MWNTs-Fe_xO_y by using MWNTs and Fe_xO_y, the Fenton-like reagent (denoted as CNIQ) was made by MWNTs-Fe_xO_y and H_2O_2. And the MWNTs-Fe_xO_y was characterized by TEM, EDS, XRD, XPS, BET, and FT-IR. Then, the CNIQ was used in the treatment of dyeing wastewater. The adsorption/degradation conditions about RhB such as the pH, the reaction temperature, the amount of MWNTs-Fe_xO_y, the amount of H_2O_2, the treatment methods, and the concentration of RhB were optimized. The characteristic results showed that many fine particles can be clearly observed on the MWNTs tube wall. The iron oxides were successfully loaded on CNTs. The adsorption experiment shows that the introduction of CNIQ can improve the adsorption ability of RhB greatly. The RhB removal rate could reach to 100% under the optimal conditions: the solid to liquid ratio is 1:2, the amount of H_2O_2 (30%) is 0.1 mL, pH is 3.58, and oscillating time is 60 min. The results also indicated that the pseudo-second-order model for RhB adsorption on MWNTs-Fe_xO_y was better than the pseudo-first-order model, and the parameters of degradation kinetics are fitted with Arrhenius equation. The degradation kinetics indicates that the linearity is good and accords with the first-order degradation kinetics. The activation energy and adsorption/degradation rate constant are 21.76 kJ/mol and 0.00047 g/(mg min), respectively, when experimental temperature is 25°C. The thermodynamic experiment indicates that the Freundlich model can well fit the adsorption of MWNTs-Fe_xO_y to RhB. This adsorption action is spontaneous and exothermic process. The removal mechanism shows that the chromogenic group phenylamino and the carbonyl bond in RhB are destroyed gradually, and the colorless organic intermediate was formed, and part of RhB can also be transformed into colorless lactone isomer, and then the colorless intermediates were degraded. This work is feasible and meaningful to use MWCNTs to remove dye.

Acknowledgments

This study was supported by YMU-DEAKIN International Associated Laboratory on Functional Materials, Key Laboratory of Resource Clean Conversion in Ethnic Region, Education Department of Yunnan Province (117-02001001002107), Scientific Research Fund Project, and Education Department of Yunnan Province (2016YJS079).

References

[1] G. Miquelard-Garnier, A. Guinault, D. Fromonteil, S. Delalande, C. Sollogoub, Dispersion of carbon nanotubes in polypropylene via multilayer coextrusion: influence on the mechanical properties, Polymer, 16 (2013) 4290–4297.
[2] M. Barmala, A.Z. Moghadam, M.R. Omidkhah, A.R. Moghadam, Increased photo-catalytic removal of sulfur using titania/MWCNT composite, J. Cent. South Univ, 23 (2016) 1066–1070.
[3] S. Simoes, F. Viana, M.A.L. Reis, M.F. Vieria, Improved dispersion of carbon nanotubes in aluminum nanocomposites, Compos. Struct., 108 (2014) 992–1000.
[4] Y.T. Xu, X.L. Peng, Y.M. Deng, G.C. Lei, Y.F. Zheng, POLY 182-Nanocomposite of polyaniline/carbon nanotube as Pt catalyst carrier for methanol electrocatalytic oxidation, Abstr. Am. Chem. Soc., 234 (2007) 234.

[5] Q. Zhang, M.Q. Zhao, J.Q. Huang, W.Z. Qian, Vertically aligned carbon nanotube arrays grown on a lamellar catalyst by fluidized bed catalytic chemical vapor deposition, Carbohydr. Chem., 47 (2009) 2600–2610.
[6] H.B. Li, J. Zhang, H.H. Jin, Q.W. Li, Separation techniques of single-walled carbon nanotubes with single electrical type and chirality, J. Phys. Chem. A, 28 (2009) 2447–2455.
[7] X. Chen, X. Zheng, X. Wang, J. Wang, Graphene/carbon nanaotube aerogel with ultra-high adsorption for the isolation of hemoglobin, Chem. J. Chinese Univ. 36 (2015) 1498–1504.
[8] M.S. Hull, A.J. Kennedy, J.A. Steevens, A.J. Bednar, C.A. Weiss Jr., P.J. Vikesland, Release of metal impurities from carbon nanomaterials influences aquatic toxicity, Environ. Sci. Technol., 43 (2009) 4169–4174.
[9] S. Skandari, A. Torabian, G.N. Bidhendi, M. Baghdadi, B. Aminzadeh, Preparation of engineered carbon nanotube materials and its application in water treatment for removal of hydrophobic natural organic matter (NOM), Desal. Wat. Treat., 57 (2016) 1–12.
[10] P.A. Tran, L. Zhang, T.J. Webster, Carbon nanofibers and carbon nanotubes in regenerative medicine, Adv. Drug. Delivery Rev., 61 (2009) 1097.
[11] M. Yang, S.J. Fang, W. Tan, B. Li, H.B. Wang, Multi-walled carbon nanotubes and matrix solid phase dispersion extraction-HPLC for the determination of acetamiprid residue in vegetables, J. Agric. Food Chem., 34 (2013) 299–301.
[12] C.X. Li, W. Tan, Y.M. Li, X.X. Hu, H.B. Wang, GC determination of residual amount of fenpropathrin in vegetable with MWCNT's-solid phase extraction, Phys. Test. Chem. Anal., 49 (2013) 709–712.
[13] C.L. Chen, X.K. Wang, M. Nagatsu, Europium adsorption on multiwall carbon nanotube/iron oxide magnetic composite in the presence of polyacrylic acid, Environ. Sci. Technol., 43 (2009) 2362–2367.
[14] H.H. Cho, B.A. Smith, J.D. Wnuk, D.H. Fairbrother, W.P. Ball, Influence of surface oxides on the adsorption of naphthalene onto multiwalled carbon nanotubes, Environ. Sci. Technol., 42 (2008) 2899–905.
[15] G. Liu, L.C. Lei, P.L. Cen, Wet air oxidation of printing and dying wastewater, J. Zhejiang Univ., 109 (2001) 235–245.
[16] C. Xing, M.L. Chen, L.C. Lan, Study on treatment of cationic dye crystal violet wastewater by flotation, J. Saf. Environ., 6 (2004) 20–22.
[17] S. Quan, Y. Zhu, Z. Ren, X. Teng, L.M. Zhu, Adsorption performance of anionic azo dye by the modified MCM-41 mesoporous molecular sieve, J. Chem. Ind. Eng., 35 (2016) 320–326.
[18] D.M. Foroughi, H. Abolghasemi, M. Esmaieli, G. Nazari, B. Rasem, Experimental study on the adsorptive behavior of Congo red in cationic surfactant-modified tea waste, Process Saf. Environ. Prot., 95 (2015) 226–236.
[19] Y. Liu, J. Zhang, J. Pan, A. Tang, Investigation on the removal of NO from SO_2-containing simulated flue gas by an ultraviolet/Fenton-like reaction, Energy Fuel, 26 (2012) 5430–5436.
[20] R.T. Guo, W.G. Pan, X.B. Zhang, J.X. Ren, Q. Jin, H.J. Xu, Removal of NO by using Fenton reagent solution in a lab-scale bubbling reactor, Fuel, 90 (2011) 3295–3298.
[21] L. Zhou, Adsorption of methylene blue on magnetic multiwalled carbon nanotube synthesized by Fenton reaction, Environ. Chem., 31 (2012) 669–676.
[22] D. Wan, W. Li, G. Wang, K. Chen, L. Lu, H. Qin, Adsorption and heterogeneous degradation of rhodamine B on the surface of magnetic bentonite material, Appl. Surf. Sci., 349 (2015) 988–996.
[23] D. Liang, J. Gao, H. Sun, P. Chen, Z. Hou, X. Zheng, Selective oxidation of glycerol with oxygen in a base-free aqueous solution over MWNTs supported Pt catalysts, Appl. Catal., B, 106 (2011) 423–432.
[24] X.Y. Zhao, Preparation and research of epoxy resin/carbon nanotubes conductive coating materials, J. B. Univ. Technol., 02 (2013) 323–332.
[25] S.J. Roosendaal, B. van Asselen, J.W. Elsenaar, A.M. Vredenberg, F.H.P.M. Habraken, The oxidation state of Fe (100) after initial oxidation in O_2, Surf. Sci., 442 (1999) 329–337.
[26] P.C.J. Graat, M.A.J. Somers, Simultaneous determination of composition and thickness of thin iron-oxide films from XPS Fe 2p spectra, Somers, Appl. Surf. Sci., 100 (1996) 36–40.
[27] J. Comyn, Practical surface analysis—by Auger and X-ray photoelectron spectroscopy, J. Electron Spectrosc. Relat. Phenom., 3 (1984) 142.
[28] T. Yamashita, P. Hayes, Effect of curve fitting parameters on quantitative analysis of $Fe_{0.94}O$ and Fe_2O_3, J. Electron Spectrosc. Relat. Phenom., 152 (2006) 6–11.
[29] M. Mazarji, B. Aminzadeh, M. Baghdadi, A. Bhatnagar, Removal of nitrate from aqueous solution using modified granular activated carbon, J. Mol. Liq., 233 (2017) 139–148.
[30] C. Ruby, B. Humbert, J. Fusy, Surface and interface properties of epitaxial iron oxide thin films deposited on MgO (001) studied by XPS and Raman spectroscopy, Surf. Interface Anal., 29 (2015) 377–380.
[31] E.F. Zegeye, E. Woldesenbet, Processing and mechanical characterization of carbon nanotube reinforced syntactic foams, J. Reinf. Plast. Compos., 31 (2012) 1045–1052.
[32] W.B. Li, H. Li, D. Wan, G. Wang, M. Wang, Y. Fu, Synthesis and characterization of pillared bentonite supported Fe_3O_4 magnetic nanoparticles composite material, J. Eng., 11 (2014) 77–81.
[33] L. Li, S. Liu, T. Zhu, Application of activated carbon derived from scrap tires for adsorption of Rhodamine B, J. Environ. Sci., 22 (2010) 1273–1280.
[34] N.G. Vakili, M. Wadhahi, A.M. Gujrathi, R.A. Maamari, M. Mohammadi, Effect of temperature and diameter of narrow single-walled carbon nanotubes on the viscosity of nanofluid: a molecular dynamics study, Fluid Phase Equilib., 434 (2017) 193–199.
[35] P. Banerjee, P. Das, A. Zaman, Application of graphene oxide nanoplatelets for adsorption of Ibuprofen from aqueous solutions: evaluation of process kinetics and thermodynamics, Process Saf. Environ. Prot., 101 (2016) 45–53.
[36] M.U. Dural, L. Cavas, S.K. Papageorgiou, F.K. Katsaros, Methylene blue adsorption on activated carbon prepared from *Posidonia oceanica* (L.) dead leaves: kinetics and equilibrium studies, Chem. Eng. J., 2011 (2011) 77–85.
[37] A.M. Puziy, O.I. Poddubnaya, A. Martínez-Alonso, F. Suárez-García, J. Tascón, Surface chemistry of phosphorus-containing carbons of lignocellulosic origin, Carbon, 43 (2005) 2857–2868.
[37] S. Horikoshi, H. Hidaka, N. Serpone, Environmental remediation by an integrated microwave/UV-illumination method. 1. Microwave-assisted degradation of rhodamine-B dye in aqueous TiO_2 dispersions, Environ. Sci. Technol., 36 (2002) 1357.
[38] F.G.D. Mendonça, M.G. Rosmaninho, P.X.D. Fonseca, R.R. Soares, J.D. Ardisson, J.C. Tristao, Use of iron and bio-oil wastes to produce highly dispersed Fe/C composites for the photo-Fenton reaction, Environ. Sci. Pollut. Res. Int., 24 (2016) 1–6.
[39] X. Wang, M. Zhou, X. Jin, Application of glow discharge plasma for wastewater treatment, Electrochim. Acta, 12 (2012) 501–512
[40] C. Wang, H. Liu, Z. Sun, Heterogeneous photo-Fenton reaction catalyzed by nanosized iron oxides for water treatment, Int. J. Photoenergy, 9 (2012) 119–135.
[41] H. Liu, Y. Wang, L. Shi, R. Xu, L. Huang, S. Tan, Utilization of reduced graphene oxide for the enhancement of photocatalytic property of TiO_2 nanotube, Desal. Wat. Treat., 28 (2016) 13263–13272.